Close Motion Estimation of UHF-RFID Tagged Objects Based on Electromagnetic Coupling

Lorenzo Bianchi, Emidio Di Giampaolo, Francesco Martinelli, and Fabrizio Romanelli

***Abstract*—We consider the close relative motion of two UHF RFID tags and the problem is the estimation of the distance between the two tags, by measuring the Received Signal Strength Indicator (RSSI) and the phase of the RFID signal backscattered by one of the two tags. Due to the short distance considered, and hence to the electromagnetic coupling between the antennas, the measured RSSI and phase present a complex and ambiguous dependence on the distance between the tags. The problem is solved through two approaches, based respectively on a Multi-Hypothesis Extended and a Multi-Hypothesis Unscented Kalman Filter (MHEKF and MHUKF). The availability of phase and RSSI allows to mitigate the ambiguity in the problem and to estimate the distance without any information on its initial value. Simulation and experimental results show the effectiveness of the approach, with the MHUKF presenting slightly better performances compared to the MHEKF. The proposed setup can be applied in manufacturing, robotics, safety and in any context where the variable distance between two close objects should be monitored.**

***Index Terms*—UHF-RFID RSSI and phase measurements, Kalman filtering, electromagnetic coupling.**

I. Introduction

PASSIVE UHF RFID tags are increasingly supporting sensing and localization functions [1], [2], [3], [4] in addition to the usual identification function. For that purpose, specific sensor functionalities are frequently included in the microchip or, as an alternative, sophisticated electromagnetic designs exploiting specific properties of the antennas [5], [6], are used. Falls within this second design methodology the use of electromagnetic coupled pairs of tags, closely spaced, which are sensitive to small reciprocal displacements. In fact, because of mutual coupling, small changes in the relative distance modify the phase and the Received Signal Strength Indicator (RSSI) of backscattered signals [7], [8], [9]. This kind of tag is conceived for structural health monitoring being able to measure (or estimate) the enlargement of cracks in structures. They require a strong electromagnetic coupling between the two tags in order to achieve high sensitivity in detecting the movement but, the stronger the coupling, the worse the communication, so a trade-off between sensing and communication needs is essential for their functioning [10], [11], [12]. In fact, the strong electromagnetic coupling between two nearby tags generates a degradation of communication due to impedance mismatch (the input impedance of each tag is strongly affected by the mutual impedance which varies with distance) and due to antenna gain variation (which generally decreases). These systems are generally used to detect small displacements typically ranging from sub-millimeters to a few tens of millimeters.

In this work we aim to extend the motion detection range to a few tens of centimeters by exploiting both mutual coupling and short-range scattering between two tags. Unlike other works [13] that try to mitigate multipath for improving localization estimation, in this work short-range scattering is deliberately used, in particular we deal with the scattering between two tags that arises at a short distance in the far field region of tag's antenna. We make use of two commercial tags deployed in close positions, as the distance between them varies while they move around the transition region between the reactive field and the far field of the tag's antenna [14]. Tags also suffer from complex coupling that alters the matching and communication properties of the two tags. That change affects the phase and the RSSI of the backscattered signals so that they have the imprinting of the distance between the two tags.

We propose an electromagnetic model of the interaction between the tags, and methods for estimating the mutual distance exploiting the information imprinted in the backscattered signals. As outlined in Section IV, this paper improves the work shown in [15] with new contributions, in particular it reports a more complete electromagnetic model of RSSI and phase of the backscattered signal, the estimate algorithms no longer require knowledge of the initial condition but exploit the measurement of the phase to make the system observable. The complexity of the new electromagnetic model has required the use of an UKF algorithm not used before while an interpolation has been introduced in the EKF. Finally, models and estimation algorithms are checked with experimental tests that, instead, are not considered in [15].

From an application point of view, the proposed method can be used both in specific contexts of structural health monitoring and in industrial robotics [16], [17], [18], where it is necessary to know the progression of the approach between

Manuscript received 29 December 2023; revised 11 February 2024 and 5 March 2024; accepted 5 March 2024. Date of publication 11 March 2024; date of current version 7 May 2024. This work was supported in part by the Italian Ministry for Research in the Framework of the Program for Research Projects of National Interest (PRIN) under Grant 2017YKXYXJ and Grant 2020RTWES4. *(Corresponding author: Emidio Di Giampaolo.)*

Lorenzo Bianchi, Francesco Martinelli, and Fabrizio Romanelli are with the Department of Civil Engineering and Computer Science, University of Rome Tor Vergata, 00133 Rome, Italy (e-mail: lorenzo.bianchi.2@uniroma2.it; francesco.martinelli@uniroma2.it; fabrizio.romanelli@uniroma2.it).

Emidio Di Giampaolo is with the Department of Industrial and Information Engineering and Economics, University of L'Aquila, I-67100 L'Aquila, Italy (e-mail: emidio.digiampaolo@univaq.it).

Digital Object Identifier 10.1109/JRFID.2024.3375795

two tagged objects for manipulation or assembly or safety. This may include (but is not limited to) the case a manipulator approaches a tagged object for grasping, a tool must perform a manufacturing operation over a tagged object in production or when controlling the approach of tagged vehicles during docking. These applications are significantly different from the ones occurring in localization scenarios since, due to the short distances involved, the coupling between the tags must be taken into account.

Different methods are reported in the literature to face each of the above mentioned applications. In particular, they make use of different technologies (e.g., vision, ultrasound, etc.) or a mix of technologies including RFID: to cite a few, [19] a manipulator robotic arm resorts to a camera and antenna RFID, [20] a system that fuses signals from a beacon emitting ultrasound chirps and RF sync signals and from RFID, [21] is based on a Synthetic Aperture Radar approach while [22] exploits near field antennas. Nevertheless that technique is not free from difficulties and complexity [23]. The synergistic use of different technologies allows mixed methods to improve the accuracy of the estimate, on the other hand they are limited in those environments in which one of the technologies used is not effective. In so-called harsh environments, for example, technologies based on vision, ultrasound or infrared are strongly disturbed by fumes, gases, dust and temperature variations. In these environmental contexts, a technology such as UHF RFID is effective as it is not affected by the disturbances that affect others. As an example of an envisaged scenario, Fig. 1 shows a sketch of the approach of a robot to a target tag by exploiting the coupling information between the target tag and a probe tag which is at a fixed distance from the reader.

The paper is organized as follows: Section II reports the problem formulation, Section III explains the used EKF and UKF to solve the problem, Sections IV and V report numerical and, respectively, experimental results. Conclusions and discussions are given in Section VI.

II. Notation and Problem Formulation

The reference scenario that we take into consideration in this work is shown in Fig. 1 in which there is a probe tag that moves back and forth relative to a target tag that is considered stationary. The movement occurs along the alignment direction of the target tag and the reader.

Let D_0 be the distance between the reader antenna and the probe tag (see Fig. 1), it is time-invariant. The distance between the probe tag and the target tag is, instead, time-variant, it will be indicated with d and is the quantity of interest to be estimated. As the probe tag approaches the target tag, the latter can be in different field regions of the probe tag as shown in Fig. 2. At the used frequencies and for the typical dimensions ℓ of a UHF tag (i.e., $10cm$) the reactive field region (having extension L_{reac}) comes to be adjacent to the far field region (L_{far}) being $L_{reac} = \lambda/2\pi \approx 2\ell^2/\lambda = L_{far}$ approximately $5cm$ (being λ the wavelength of the signal corresponding to the used frequency of 867 MHz). The interaction between the probe tag and the target

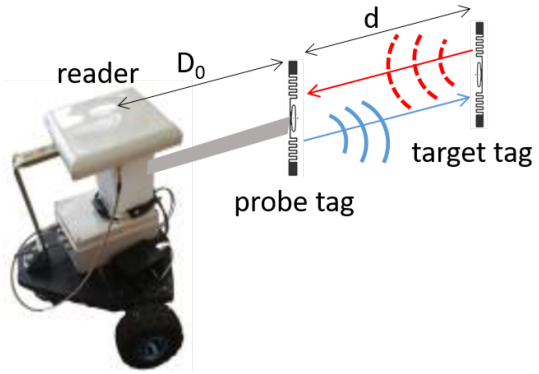

Fig. 1. The considered setup with relevant distances.

tag therefore passes from an exchange of reactive energy when $d < L_{reac}$ to a short-range scattering in which one of the two tags partially reflects the electromagnetic wave towards the other creating interference with the wave that arrives directly from the reader. The transition from the reactive field coupling to the scattering coupling is evidently not clear but there is a superposition of the two effects when the distance d is close to L_{reac}.

In this situation, an electromagnetic model capable of describing the variation of the signal backscattered by the tags must take into account both the change in the parameters of antennas (i.e., input impedance and gain) due to reactive interactions when d is very short and the multipath between tags when d is in the far field region. The modeling of reactive interactions can be done as shown in [10] after the determination of self and mutual impedance of the couple of tags for different values of d that can be achieved with a numerical analysis of a detailed electromagnetic model of tags' antennas. Nevertheless, the complexity and the numerical nature of that model make it not suitable to be integrated into a Kalman filter in which closed-form equations are preferable being computationally much less demanding (e.g., EKF requires the derivatives (w.r.t. d) of the measurement model for the calculation of the Jacobian matrix). For this reason, we resort to interpolating functions as reported in Section III-A to account for the effects of reactive interaction on the RSSI and on the phase of the backscattered signal.

Far-field interaction instead can be modeled with the equation of a multipath channel

$$E^i(d) = V_0 \frac{e^{-j\beta D_0}}{(4\pi D_0)} CH(d), \tag{1}$$

where V_0 is a complex amplitude while $E^i(d)$ is the electric field impinging on the probe tag, it is the superposition of the field $V_0(e^{-j\beta D_0}/[(4\pi D_0)])$ coming from the reader antenna after propagating the distance D_0 and the field reflected by the target tag which travels an additional path of length $2d$. It is modeled using the channel response

$$CH(d) = \left[1 + \Gamma \frac{e^{-j2\beta d}}{\left(1 + \frac{d}{D_0}\right)d}\right]$$

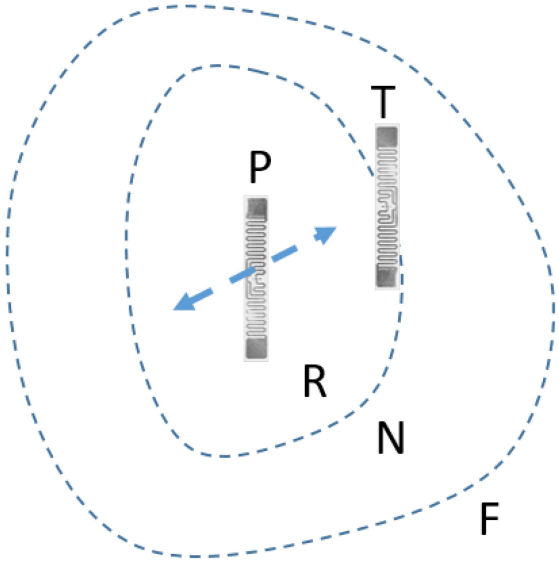

Fig. 2. Schema of tag's antenna field zones: R reactive field region; N radiative near field region; F far field region. P probe tag, T target tag.

with $\Gamma = \Gamma_0 e^{j\Phi_0}$ a factor that accounts for reflection of the target tag having Γ_0 and Φ_{Γ_0} as magnitude and phase, respectively while $\beta = (2\pi/\lambda)$ is the propagation factor.

The RSSI of the RFID signal backscattered by the probe tag and measured by the reader changes with the distance d (and on D_0 as well) according to the following equation:

$$RSSI(dBm) = RSSI_0 + 20\log_{10}\left(|CH(d)|^2\right) + n_{RS}, \qquad (2)$$

where $RSSI_0$ is depending on D_0 and on the properties of reader and tags antennas while $n_{RS} \sim \mathcal{N}(0, \sigma_{RS}^2)$ is a measurement error.

Similarly, the phase of the signal backscattered from the probe tag and measured at the reader is

$$\phi = mod\left(-2\beta D_0 + 2\arg\left[CH(d)\right] + \phi_0 + n_\phi, \pi\right) \qquad (3)$$

with ϕ_0 a phase offset depending on the particular setup and $n_\phi \sim \mathcal{N}(0, \sigma_\phi^2)$ a measurement error.

Assuming zero noise (i.e., $n_{RS} = 0$ and $n_\phi = 0$), the RSSI model of measurements as a function of d is reported in Fig. 3 while the phase is shown in Fig. 4. These figures have been obtained by applying, respectively, the measurement models (2) and (3) with the following set of parameters: $D_0 = 1.0$ m, $RSSI_0 = -59.68$ dBm, $\beta = 2\pi/\lambda = 18.16\ m^{-1}$, $\Gamma_0 = 0.02$ and $\Phi_{\Gamma_0} = 0.8416$. If only the RSSI or only the phase is considered, the ambiguity of the information on the distance d between the two tags is evident. The ambiguity is mitigated by exploiting the combination of the RSSI and phase measurements. Similarly to the antenna parameters in the reactive zone, the parameter Γ is not known a priori depending on the particular tag, so the model has to be tuned with preliminary measurements.

III. Solution Approach

Two solution approaches are proposed in this paper: the first one is based on an Extended Kalman Filter (EKF), while the other one relies on an Unscented Kalman Filter (UKF, [18]). The UKF is a filtering approach expressly designed to cope with nonlinear systems and, without introducing a linearization of the dynamics and of the measurement model of the system, usually provides quite better performances than the EKF, without a significant increment in the computational complexity. In our case, the main reason to consider the UKF is the complexity of the highly nonlinear measurement model. This makes the linearization a quite poor approximation of the true model (which works only in the close proximity of the true value of the distance). Moreover, the complexity of the model does not allow to obtain a simple analytical expression of the Jacobian matrix required to apply the EKF. For this reason, the EKF has been applied by computing the Jacobian of an interpolated measurement model, as detailed in Section III-A. On the contrary, the UKF, which computes the expected measurements on a set of properly selected points (called *Sigma Points*), does not require the evaluation of the derivatives of the measurement model and thus uses the exact model. In both cases, a multi-hypothesis filter is considered (MHEKF and MHUKF in the case of the EKF and, respectively, of the UKF) to cope with the fact that the initial distance is not known and more instances of the filter are initialized with a different distance estimate. In fact, even if in some situations the UKF presents better convergence

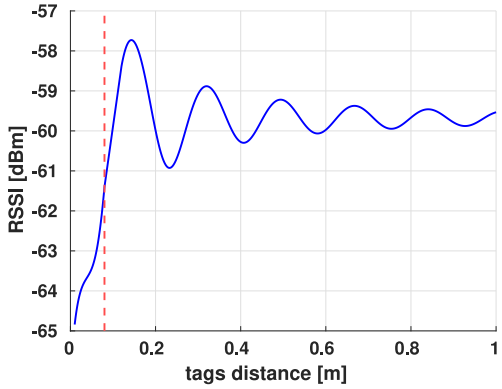

Fig. 3. The RSSI of the backscattered RFID signal as a function of the distance d between the two tags. The vertical dashed line shows the border between the reactive field model and the far field model.

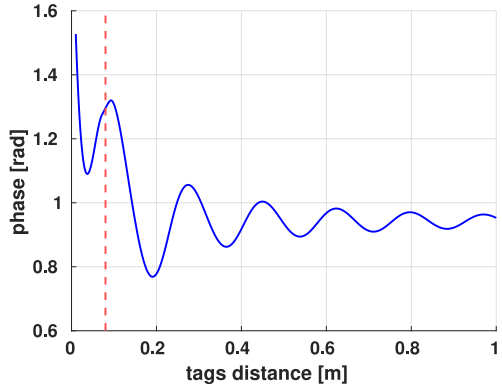

Fig. 4. The phase of the backscattered RFID signal as a function of the distance d between the two tags. The vertical dashed line shows the border between the reactive field model and the far field model.

properties with respect to the EKF, both approaches do not converge if the initial distance estimate is too far from the true value of the distance.

A. Multi Hypothesis Extended Kalman Filter (MHEKF)

The proposed filter, using the available measurements (the RSSI and the phase shift of the RFID signal), provides an estimate of the distance d and of the (scalar) velocity $v = \dot{d}$ of the target tag with respect to the probe tag. The state x of the filter is then $x = [d, v]^T$. As shown in [15], the necessity of estimating also the velocity v depends on the fact that, in the implementation of the prediction step of the filter, no internal measurements of the tag motion (like the ones coming from, e.g., inertial sensors) is assumed available in this setup. This, together with the ambiguity in the RSSI and in the phase measurements, may result, if the velocity is not included in the estimation, in a poor performance of the filter.

We will present, at first, the structure of a single instance of the EKF, by leaving at the end of the section the description of the MHEKF, which uses a certain number of EKF instances, each one initialized with a different initial condition. The EKF comprises a prediction and a correction step. Since, as mentioned, no direct internal measurement of the tag motion is available at this stage, the prediction step is designed by assuming a rough knowledge of the expected rate which characterizes the variation of the velocity v. The prediction step can be obtained by considering the discretized dynamics of the system, which in matrix form, with a sampling time Δ_T, can be written as follows:

$$x_{k+1} = Ax_k + \omega_k, \tag{4}$$

where $x_k = [d_k, v_k]^T$, A is a 2×2 matrix with $A(1,1) = A(2,2) = 1$, $A(1,2) = \Delta_T$ and $A(2,1) = 0$ and finally $\omega_k = [0, a_k\Delta_T]^T$, being a_k the (unknown) acceleration at time step k (i.e., $a = \dot{v}$). Being unknown, $a_k\Delta_T$ will be modeled as a Gaussian random variable n_{Δ_v} with 0 mean and standard deviation $\sigma_{\Delta v}$. The size of the standard deviation $\sigma_{\Delta v}$ is assigned taking into account the expected changing rate of the velocity. It is now possible to write the prediction step of the EKF:

$$\hat{x}^-_{k+1} = A\hat{x}_k, \tag{5}$$

$$P^-_{k+1} = AP_kA^T + Q_k, \tag{6}$$

where $\hat{x}^-_{k+1}$ is the a priori estimate provided by the filter, P_k is the covariance matrix and Q_k is a 2×2 matrix with all 0 elements apart from $Q(2,2) = \sigma^2_{\Delta v}$.

The correction step of the filter performs a correction of the predicted estimate by considering the measurement vector z_{k+1}, which comprises the *RSSI* and the phase shift ϕ in the RFID signal observed at time step $k+1$:

$$z_{k+1} = \begin{bmatrix} RSSI_{k+1} \\ \phi_{k+1} \end{bmatrix}, \tag{7}$$

where *RSSI* and ϕ are respectively given by (2) and (3). The expected measurement vector at this stage will be denoted by $\hat{z}^-_{k+1} = h(\hat{x}^-_{k+1})$ and will comprise the expected RSSI and phase measurements, which can be computed using respectively (2) and (3), considering zero noise, with the distance estimated in the prediction step. The correction step can then be written as follows:

$$\hat{x}_{k+1} = \hat{x}^-_{k+1} + K_{k+1}\left(z_{k+1} - \hat{z}^-_{k+1}\right), \tag{8}$$

$$P_{k+1} = (I - K_{k+1}H_{k+1})P^-_{k+1}. \tag{9}$$

In this expression I is the 2×2 identity matrix, $K_{k+1} = P^-_{k+1}H^T_{k+1}(H_{k+1}P^-_{k+1}H^T_{k+1} + R)^{-1}$ is the Kalman gain, with H_{k+1} the Jacobian of the measurement model and

$$R = \begin{bmatrix} \sigma^2_{RSSI} & 0 \\ 0 & \sigma^2_{\phi} \end{bmatrix} \tag{10}$$

being the covariance matrix of the noise in the RSSI and the phase measurements. More in detail, H_{k+1} is a 2×2 matrix, where the first row contains the derivative of the *RSSI* measurement in (2) with respect to the estimated variables d and v, evaluated at $\hat{d}^-_{k+1}$ and $\hat{v}^-_{k+1}$. Similarly, the second row of H_{k+1} contains the derivative of the phase in (3) with respect to d and v, still evaluated at $\hat{d}^-_{k+1}$ and $\hat{v}^-_{k+1}$. Since the RSSI and the phase only depend on the distance d and are independent of the velocity v, $H_{k+1}(1,2) = H_{k+1}(2,2) = 0$.

Since it is not straightforward to obtain a closed-form expression of the measurement model derivative in (2) and (3) with respect to d (needed in the computation of the Jacobian H_{k+1}), we have decided to compute this derivative by introducing an approximate measurement model, obtained through MATLAB's *interp*1 function using "spline" as the method parameter. By doing so, we obtain a struct from which the derivative function can easily be computed. Moreover, if *interp*1 receives a dense interval of points as input, the resulting interpolation function is almost identical to the actual model. It is important to note that the interpolated derivative function is used only inside the EKF computations, as the expected RSSI and phase are still obtained through the complex model equations.

Since in this paper the initial value of the distance is assumed unknown and the EKF may diverge if the initial estimate is not assigned sufficiently close to the true value of d, a MHEKF is proposed to solve the problem. In this case, different EKF instances are introduced, each one initialized with a different distance d (but all with a zero velocity and a proper standard deviation σ_{v_0}, to cope with the uncertainty in the initial velocity). As a result, the interval of all possible initial distances $[0, D_{max}]$ is partitioned into a set of small segments, and an EKF is initialized in each segment, with a standard deviation σ_{d_0} which depends on the size Δ_s of each one of these small segments (i.e., $\sigma_{d_0} = \Delta_s/6$). With this initialization, the initial covariance matrix P_0 of each instance will be a diagonal 2×2 matrix with diagonal elements $\sigma^2_{d_0}$ and $\sigma^2_{v_0}$. The EKF instances run in parallel but, at each time step k, the one with the largest weight is selected to produce the estimate $\hat{x}_k$. The weight is computed by taking into account the agreement of the expected measurements of the filter with the true measurements. By denoting with $w^{(\ell)}_k$ the weight at

time step k of instance ℓ, whose initial value is $w_0^{(\ell)} = 1$, at each step it is updated through the following equation:

$$w_{k+1}^{(\ell)} = w_k^{(\ell)} \cdot \exp\left\{-\frac{1}{2}\Delta z_{k+1}^T \Pi \Delta z_{k+1}\right\}, \tag{11}$$

being $\Pi = (H_{k+1}P_{k+1}^- H_{k+1}^T + R)^{-1}$, $\Delta z_{k+1} = z_{k+1} - \hat{z}_{k+1}$ the difference between true and expected measurement at instance ℓ and all quantities H, P and $\hat{z}$ referred to instance ℓ. Finally, the weights are normalized to one. The use of an exponential function in (11) often leads to instances' weights that differ from each other by many orders of magnitude, also in the case of non-diverging EKFs. Therefore, in order to have more similar weights, it is possible to transform (11) by applying the logarithmic function to both sides of the equation. The resulting formula, this time with the initial condition $\bar{w}_0^{(\ell)} = 0$, then becomes:

$$\bar{w}_{k+1}^{(\ell)} = \bar{w}_k^{(\ell)} - \frac{1}{2}\Delta z_{k+1}^T \Pi \Delta z_{k+1}. \tag{12}$$

B. Multi Hypothesis Unscented Kalman Filter (MHUKF)

The structure of the MHUKF coincides with the one of the MHEKF described in Section III-A, i.e., same initialization of the different instances and same selection of the instance with the largest weight to produce the current estimate. In the MHUKF however, each instance is an UKF, with a different prediction and correction step, which are detailed in this section. Also, the equation to update the weight of the different UKF instances is slightly different from the one reported in (11) and will be described below.

The UKF is based on the generation of a set of $2n_a+1$ Sigma Points ξ_i, $i = 0, 1, \ldots, 2n_a$, being n_a the dimension of the augmented state x_a of the system, which in this case comprises the vector x of the estimated variables and the process noise variable n_{Δ_v}. Hence we have $n_a = 3$ and $x_a = [x^T, n_{\Delta_v}]^T$. In the UKF x_a is described through a Gaussian random variable with mean $m_a = [m_x^T, 0]^T$, being m_x the mean of x and being 0 the mean of n_{Δ_v}. Accordingly, the covariance matrix of x_a is a 3×3 diagonal matrix P_a with the first 2×2 block given by the covariance matrix P of x and the element $(3, 3)$ given by $\sigma_{\Delta v}^2$. Let

$$[\xi_i, \omega_i] = SP(m_a, P_a)$$

be the procedure (detailed in [18]) to generate the $2n_a + 1$ Sigma Points $\xi_i \in \mathbb{R}^{n_a}$, and their weights ω_i, corresponding to the Gaussian variable x_a.

In the prediction step of the UKF, we first generate the Sigma Points (and their weights) from the estimate obtained in the previous step:

$$\left[\xi_{i,k}, \omega_{i,k}\right] = SP\left(\left[\hat{x}_k^T, 0\right]^T, diag(P_k, \sigma_{\Delta v}^2)\right). \tag{13}$$

Then, the discrete dynamics equation (4) is applied to each Sigma Point as follows:

$$\xi_{i,k+1}^- = A_a \xi_{i,k}, i = 0, 1, \ldots, 2n_a. \tag{14}$$

Here $A_a = [A, B]$, with $B = [0, 1]^T$ and $\xi_{i,k+1}^- \in \mathbb{R}^2$ is the value of x corresponding to the i-th Sigma Point after the transformation dictated by the dynamics. The predicted estimate of x and its covariance matrix at time step $k + 1$ are then given by:

$$\hat{x}_{k+1}^- = \sum_{i=0}^{2n_a} \omega_{i,k} \xi_{i,k+1}^-, \tag{15}$$

$$P_{k+1}^- = \sum_{i=0}^{2n_a} \omega_{i,k} \left(\xi_{i,k+1}^- - \hat{x}_{k+1}^-\right)\left(\xi_{i,k+1}^- - \hat{x}_{k+1}^-\right)^T. \tag{16}$$

The correction step of the filter is as follows. First of all we compute the measurement $\mathcal{Z}_{i,k+1}^-$ expected in each Sigma Point $\xi_{i,k+1}^-$ according to the measurement model:

$$\mathcal{Z}_{i,k+1}^- = h\left(\xi_{i,k+1}^-\right).$$

The expected measurement at this stage is then obtained by averaging over the $\mathcal{Z}_{i,k+1}^-$:

$$\hat{z}_{k+1}^- = \sum_{i=0}^{2n_a} \omega_{i,k} \mathcal{Z}_{i,k+1}^-.$$

This allows to compute the innovation Δz_{k+1} and the covariance matrices $P_{zz,k+1}$ and $P_{xz,k+1}$ needed in the update process of the filter as follows:

$$\Delta z_{k+1} = z_{k+1} - \hat{z}_{k+1}^-,$$

where z_{k+1} is the actual measurement (RSSI and phase) obtained at time step $k + 1$,

$$P_{zz,k+1} = \sum_{i=0}^{2n_a} \omega_{i,k} \left(\mathcal{Z}_{i,k+1}^- - \hat{z}_{k+1}^-\right)\left(\mathcal{Z}_{i,k+1}^- - \hat{z}_{k+1}^-\right)^T + R$$

and

$$P_{xz,k+1} = \sum_{i=0}^{2n_a} \omega_{i,k} \left(\xi_{i,k+1}^- - \hat{x}_{k+1}^-\right)\left(\mathcal{Z}_{i,k+1}^- - \hat{z}_{k+1}^-\right)^T.$$

The estimate (and its covariance matrix) is then corrected as follows:

$$\hat{x}_{k+1} = \hat{x}_{k+1}^- + K_{k+1}\Delta z_{k+1} \tag{17}$$

$$P_{k+1} = P_{k+1}^- - K_{k+1} P_{zz,k+1} K_{k+1}^T, \tag{18}$$

with

$$K_{k+1} = P_{xz,k+1}\left(P_{zz,k+1}\right)^{-1}.$$

Each UKF instance ℓ executes the prediction and the correction steps just described producing an estimate $\hat{x}_k^\ell$. The MHUKF selects the instance ℓ with the largest weight. The weight w_{k+1}^ℓ of each instance ℓ is computed according to the following equation:

$$w_{k+1}^{(\ell)} = w_k^{(\ell)} \cdot exp\left\{-\frac{1}{2}\Delta z_{k+1}^T \left(P_{zz,k+1}\right)^{-1} \Delta z_{k+1}\right\}. \tag{19}$$

The weights are then normalized to one. As already done for the EKF, the previous equation is simplified by applying a logarithm function to both equation members and by updating the initial condition from 1 to 0. Thus, Eq. (19) becomes:

$$\bar{w}_{k+1}^{(\ell)} = \bar{w}_k^{(\ell)} - \frac{1}{2}\Delta z_{k+1}^T \left(P_{zz,k+1}\right)^{-1} \Delta z_{k+1}. \tag{20}$$

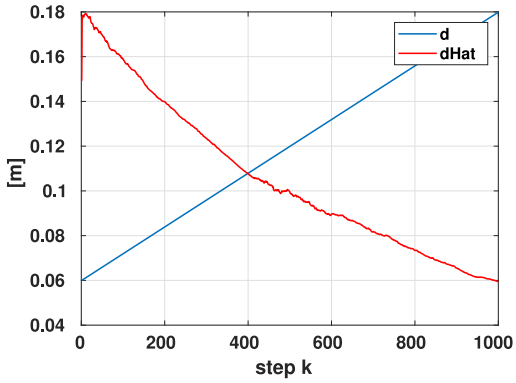

Fig. 5. Estimation ambiguity: the trajectory estimated with the approach in [15] when starting from a far initial condition with the same RSSI measurement.

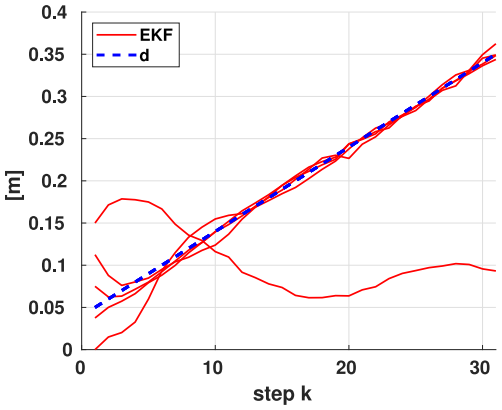

Fig. 6. EKF's distance estimate when using both RSSI and phase measurements starting from different initial conditions.

IV. Numerical Results

A. Limitations of the Previous Approach in [15]

The algorithm presented in [15] gives a proper distance estimate only when initialized around the actual starting position. On the contrary, the estimate could diverge, or worse, converge to a wrong trajectory, whose weight score (12) was, sometimes, even greater than the weight of the EKF instance initialized close to the true distance and producing a correct estimate.

Let us consider the RSSI model and the algorithm from [15] with a high density of measurements, only possible in simulation. Let the starting position of the target tag be at about 6 *cm* from the tag probe, corresponding to an RSSI measurement of -61 *dBm*; nonetheless, the same measurement may also be obtained from an initial distance of about 18 *cm*. An EKF initialized at 15 *cm* produces a plot as in Fig. 5, where the estimate converges immediately to the closer distance producing the measured RSSI, 18 *cm*. The ground truth, the blue line, indicates a movement of the robot that makes it go away from the fixed tag, while the estimated distance, in red, suggests an approach. This makes sense as the measurements obtained from the two initial points, moving the opposite directions, are the same.

To fix this issue, it is necessary to add a further measurement, the phase of the signal, which allows to eliminate the ambiguity. Using these two sources of information, not only it is possible to have an estimated trajectory whose weight is low when the initial condition is too far from the actual one (and the obtained estimate is not correct), but also to have a wider basin of attraction. The basin of attraction is the set of all the initial estimates that allow to obtain convergence of the filter to the true distance. As depicted in Fig. 6, it consists of the segment $(0, 10\ cm)$ around the true initial distance (5 *cm* in the figure). It can be observed that the estimate initialized in 15 *cm* is too far from the true value (about 10 *cm*), i.e., it is outside the attraction basin and does not allow to obtain the convergence of the estimate to the true value.

Without loss of generality (since this simply corresponds to a suitable scaling of the involved variables), a sampling time $\Delta_T = 1$ is assumed and, therefore, the tag velocity v_k only depends on the step dimension Δ_d, being equal to 1 cm/s if $\Delta_d = 1\ cm$. By step dimension Δ_d we denote the difference $d_{k+1} - d_k$ between the distances in two consecutive steps of the simulation. Considering a number of instances $n_f = 5$ with initial conditions equally distributed inside the interval going from $d_{min} = 0\ m$ to $d_{max} = 0.15\ m$, the standard deviations used for this EKF test are $\sigma_{d_0} = (d_{max} - d_{min})/n_f/6$, $\sigma_{v_0} = 10^{-6}\ m/s$, $\sigma_{\Delta v} = 10^{-3}\ m/s$, $\sigma_{RSSI} = 0.5\ dBm$ and $\sigma_\phi = 10°$. In Fig. 6, the not converging instance with the initial condition at 0.15 *m*, resembling the estimated curve in Fig. 5, is purposely shown. In this case, the weight of this instance is extremely lower compared to the one of the other converging instances.

B. Interpolation of the Measurement Model and Introduction of the UKF

With the introduction of the new model described in Section II, more complex than the one considered in [15], it is no longer possible to compute a closed-form derivative equation to be fed to the linearized model of the EKF algorithm. Two different solutions are implemented to solve such a problem: the new model is interpolated using spline functions, making it possible to compute its derivatives; the second solution deals with the implementation of an UKF algorithm, which does not need the model to be linearized. Fig. 7 shows the UKF's convergence region computed with EKF's same values. Checking both Fig. 6 and Fig. 7 it is easy to note that they have a similar basin of attraction even though, for small values of the step dimension Δ_d (e.g., the one used in [15]), the UKF is characterized by a larger basin of attraction.

C. Effect of the Measurements' Density

To perform tests with real-world measurements it is necessary to understand the effects of the step dimension Δ_d on the estimation error, and if the minimum step that is physically achievable in the laboratory allows to obtain good results. To do this, a simulation on a fixed path (with a distance between tags going from 5 *cm* up to 50 *cm*) is set up: the step dimension is tested inside the interval $[0.1, 5]$ *cm* producing, consequently, a tag velocity spanning from 0.1 cm/s to 5 cm/s;

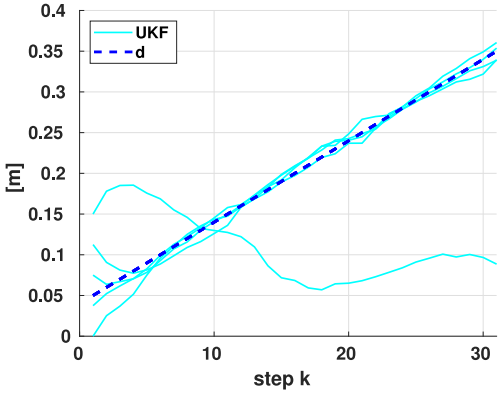

Fig. 7. UKF's distance estimate when using both RSSI and phase measurements starting from different initial conditions.

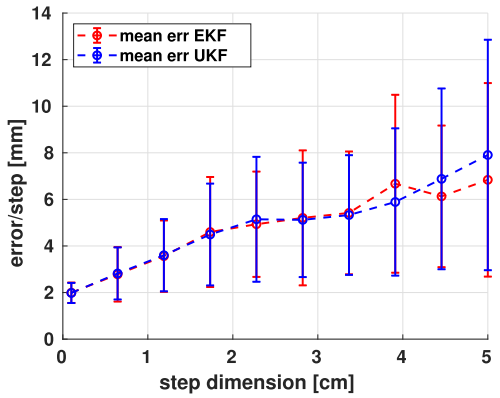

Fig. 8. Normalized error trend as step dimension varies.

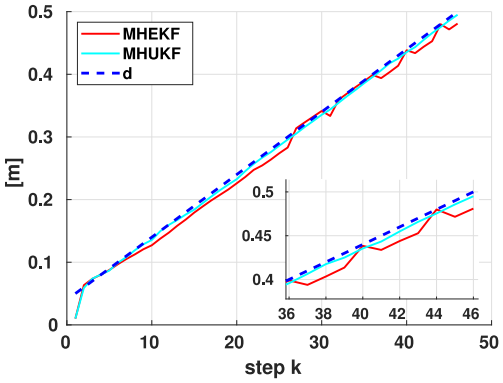

Fig. 9. Final trajectory fusing best segments estimated by all the instances.

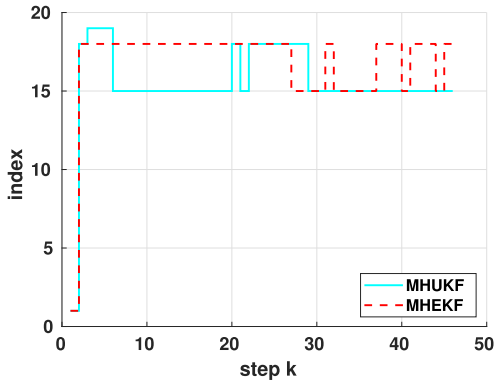

Fig. 10. Instance index selected in each step of the simulation reported in Fig. 9.

in order to minimize the randomness of the results, a total of 400 simulations starting from the actual initial distance are performed for each step dimension and their errors are averaged; as the number of simulation steps differs among the various tests because of the fixed length path, the error derived by each test is normalized using the total number of steps. Fig. 8 shows how the error per step decreases by decreasing the step dimension, meaning that the only constraint on this value depends on the ability to take measures with the real equipment.

D. Fusing Instances

As explained in Section III, when running both an MHEKF or MHUKF, there is the need to understand which running instance is the one providing the best estimate. This is obtained by considering the weight of each instance which is computed according to Eqs. (12) and (20) for the MHEKF and the MHUKF respectively. It is possible to work both in an offline and online way: the first one consists of choosing the instance that has the largest weight at the end of the simulation. On the other hand, the online process is about comparing all weights at each step and selecting the best one in order to produce an estimated trajectory being the fusion of all instances results. Fig. 9 shows both the EKF's and UKF's trajectories produced by switching instances as suggested in Fig. 10. In this plot the red line, the EKF, has a more jumping behavior compared to the UKF, which instead is always closer to the ground truth, and its jumps are not noticeable in this test.

E. Fused Trajectories Error

The test in Fig. 8 has been repeated considering the complete MHEKF and MHUKF algorithms, showing how the step dimension Δ_d influences the error per step. In this case, we repeated 50 times the simulation for Fig. 9 with $n_f = 50$ instances. Each instance has an initial condition taking value inside the interval described by $d_{min} = 0.01\ m$ to $d_{max} = 0.15\ m$, and standard deviations $\sigma_{d_0} = (d_{max} - d_{min})/n_f/6$, $\sigma_{v_0} = 10^{-2}\ m/s$, $\sigma_{\Delta v} = 10^{-4}\ m/s$, $\sigma_{RSSI} = 0.5\ dBm$ and $\sigma_\phi = 10°$. Comparing Figs. 8 and Fig. 11 it can be noted that the error per step is generally lower in the former case, as the trajectories used to compute the average have all the initial conditions equal to the actual starting distance.

F. Trajectory With Piecewise Constant Slope

In this section, the developed algorithms are tested on a slightly more complex trajectory made up of three piecewise constant slope segments: the first one is similar to the trajectory used so far, in which the tag probe moves away from the fixed tag; the second segment has a zero velocity with the tag stationary for some time; at last, the tag probe goes back to the starting position moving slower than it did in the first segment.

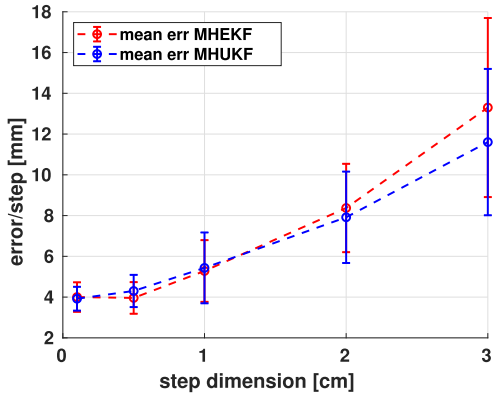

Fig. 11. Error per step as a function of the step dimension with the complete MHEKF and MHUKF algorithms (and unknown initial condition).

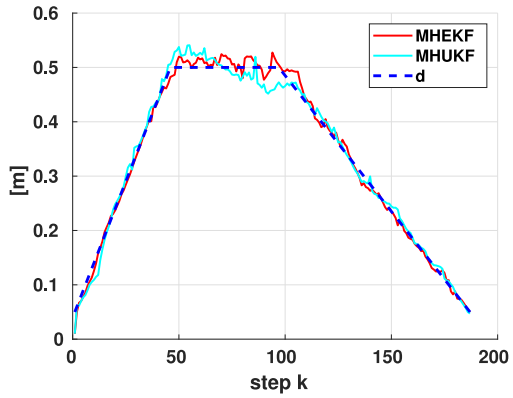

Fig. 12. MHEKF and MHUKF estimated trajectories made up of segments coming from the best instance at each time step.

Assuming that all instances have an initial condition inside the interval spanning from $d_{min} = 0.01\ m$ to $d_{max} = 0.2\ m$ and there are a total of $n_f = 200$ instances, this last test is performed using the following standard deviation values:

- $\sigma_{RSSI}^{EKF} = \sigma_{RSSI}^{UKF} = 0.5\ dBm$,
- $\sigma_{\phi}^{EKF} = \sigma_{\phi}^{UKF} = 10°$,
- $\sigma_{d_0}^{EKF} = \sigma_{d_0}^{UKF} = (d_{max} - d_{min})/n_f/6$,
- $\sigma_{v_0}^{EKF} = 10^{-3}\ m/s$,
- $\sigma_{v_0}^{UKF} = 10^{-4}\ m/s$,
- $\sigma_{\Delta v}^{EKF} = 10^{-3}\ m/s$,
- $\sigma_{\Delta v}^{UKF} = 5 \cdot 10^{-4}\ m/s$.

Fig. 12 shows how the estimate evolves in time compared to the ground truth. MHUKF has more difficulties in following the correct trajectory when the velocity changes instantaneously at step $k = 50$ and stays constant for some time.

The best indexes that maximize (12) and (20) at each step are depicted in Fig. 13. With such a trajectory, it is worth noting that weights do not always give the best segments at each time step. Fig. 14 represents the trajectory produced with the best segments at each time step obtained during another test (the jumps among instances are depicted in Fig. 15). Here it can be seen that, right after the start of the descent, both filters seem to diverge for some steps before returning to the correct trajectory. On the other hand, Fig. 16 shows, for the same test, the paths estimated by the instances whose weights

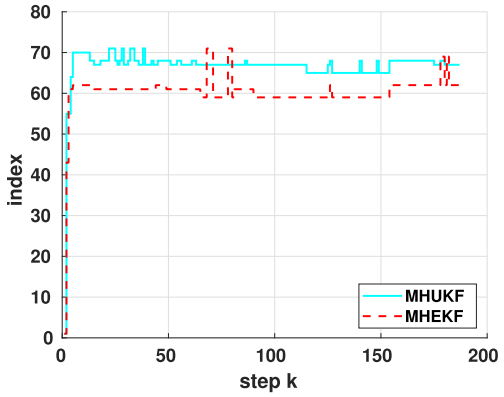

Fig. 13. Instance indexes that maximize weights at each time step.

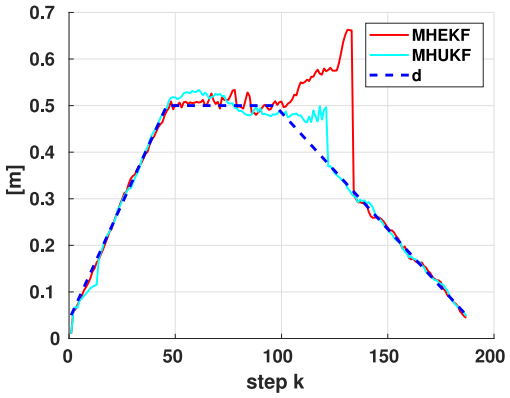

Fig. 14. Example where the abrupt change in the velocity v yields large estimation errors.

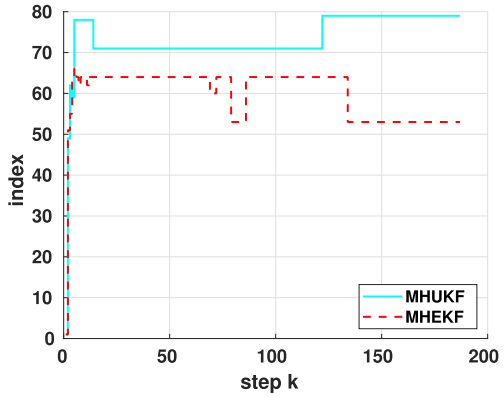

Fig. 15. Instance indexes selected in the simulation reported in Fig. 14.

are the highest at the end of the simulation, and, in this case, the overall trajectories have no diverging problems.

V. Experimental Tests

Some experiments with real measures have been performed using the LabID UH105 as tags [24] and the Thing Magic M6e with 6 dB gain circular polarized antenna as reader. The experimental setup is shown in Fig.17: a sliding rod having a submillimeter step moves the target tag placed over a cardboard box while the probe tag is attached over a styrofoam column. The system parameters are exactly the ones

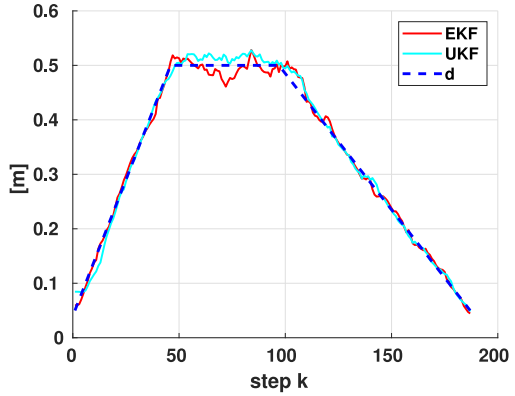

Fig. 16. Trajectory of the instance whose weight is the highest at the end of the simulation.

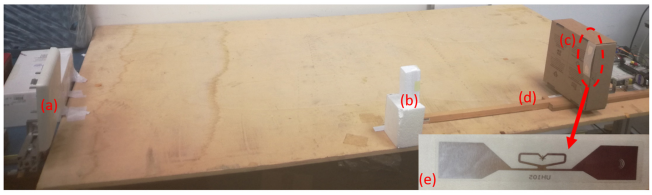

Fig. 17. Experimental setup: (a) reader's antenna; (b) probe tag; (c) target tag; (d) sliding rod; (e) used tag.

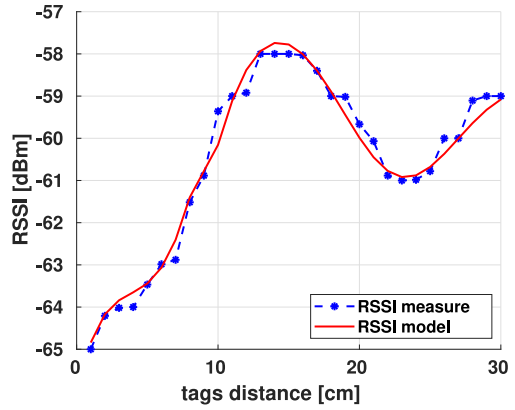

Fig. 18. Comparison between RSSI measures and model.

considered in Section II to generate Figs. 3 and 4, in particular the distance D_0 between fixed tag and reader's antenna is equal to 1 m.

A. First Test

The first experiment consists of 25 measures taken with a distance between tags spanning from 0.04 m up to 0.28 m. Figs. 18 and 19 show the comparison between the model and the measures and they are, as expected, quite similar but non exactly matching, due to imperfections in the model characterization and experimental errors. Since the interaction between the two tags dampens as the distance d between the tags increases, we limited d to 30 cm because for larger distances the RSSI and phase become little variable.

Running the algorithms on these data produces the results plotted in Fig. 20. The values used for this test, for both MHEKF and MHUKF, are:

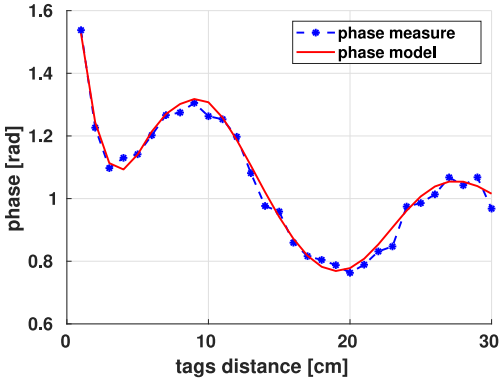

Fig. 19. Comparison between phase measures and model.

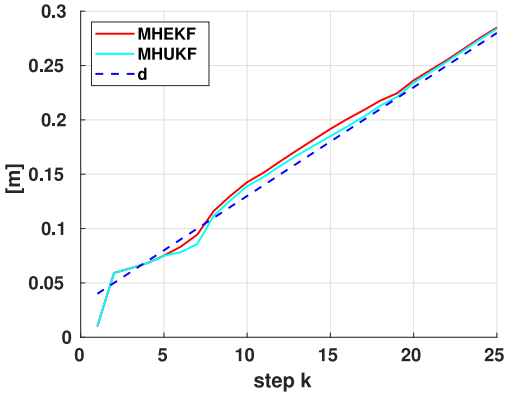

Fig. 20. MHEKF and MHUKF estimated trajectory with real-world measures.

- $d_{min} = 0.01\ m$,
- $d_{max} = 0.2\ m$,
- $n_f = 50$,
- $\sigma_{RSSI} = 0.1\ dBm$,
- $\sigma_\phi = 0.2°$,
- $\sigma_{d_0} = (d_{max} - d_{min})/n_f/6$,
- $\sigma_{v_0} = 3 \cdot 10^{-4}\ m/s$,
- $\sigma_{\Delta v} = 3 \cdot 10^{-5}\ m/s$.

The trajectories obtained have errors per step equal to $e^{MHEKF}_{step} = 8.58\ mm$ and $e^{UKF}_{step} = 6.43\ mm$. The measures are collected with a step dimension of 1 cm meaning that, taking as a reference the plot in Fig. 11, the error per step obtained with real values is about 1.5 times greater than the simulation error.

B. Second Test

The second experimental test we propose is similar to the simulation in Fig. 12, where the tag moves away from the reader and then goes back to the initial position. As in the first case, we have taken 25 measures with a step dimension of 1 cm from 0.04 m up to 0.28 m and 24 more from 0.27 m to 0.04 m, for a total of 49 measurements. Almost all parameters are the same as in the previous case, except for σ_{v_0} and $\sigma_{\Delta v}$, which now are respectively equal to $1 \cdot 10^{-3}\ m/s$ and $3 \cdot 10^{-3}\ m/s$. Fig. 22 shows that both MHEKF and MHUFK have some more difficulties in following the backward trajectory, but the maximum error obtained by both algorithms is about 5 cm

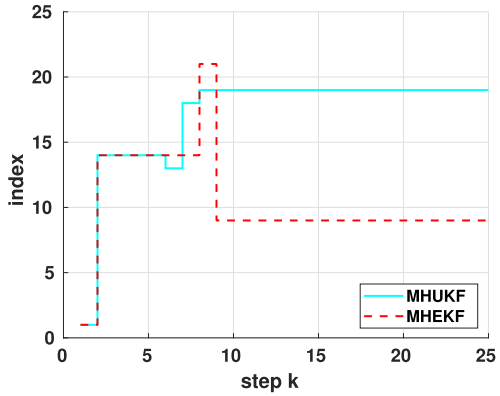

Fig. 21. Instance index selected by the MHEKF and the MHUKF with the real-world measures.

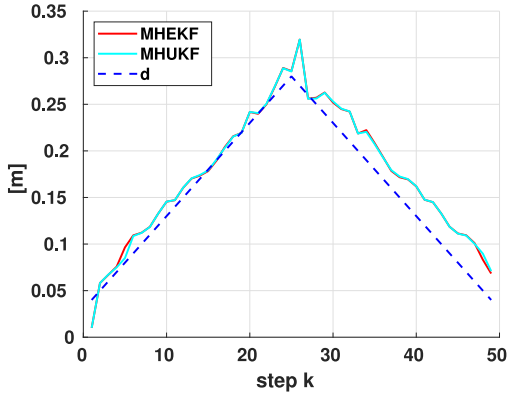

Fig. 22. MHEKF and MHUKF estimated trajectory with real-world measures when moving the tag back and forth.

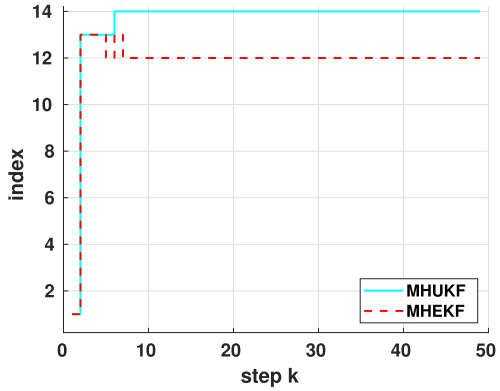

Fig. 23. Instance index selected by the MHEKF and the MHUKF with the real-world measures when moving the tag back and forth.

at step 26, that is when the trajectory changes direction. The errors per step in this second experiment are 18.13 *mm* for the MHEKF and 18.03 *mm* for the MHUKF. According to this test, it is possible to observe that the filter is able to capture the backward movement, even if the estimation error is larger than the one observed in the forward motion.

VI. Conclusion

The problem of estimating the distance between two tags in close relative motion has been considered in this paper. A Multi-Hypotheses Extended and a Multi-Hypotheses Unscented Kalman Filter have been used to solve the problem by exploiting the measurement of the RSSI and of the phase of the RFID signal backscattered by one of the tags. The short distance introduces an electromagnetic coupling between the antennas in such a way that the dependence of the RSSI and of the phase on the distance is ambiguous and is described through a complex model. The necessity of using Multi-Hypotheses filters is motivated by the fact that the initial value of the distance is assumed unknown and an EKF (or an UKF) converges to the true distance only if it is initialized in a small neighborhood of the true initial value. For this reason, several EKF and UKF instances are initialized with different initial conditions: the one with the largest agreement with measurements is selected by the Multi-Hypotheses filter to produce the correct distance estimate. It has been observed that the convergence of the filter can be attained in general only if using both RSSI and phases, which mitigate the ambiguity of the measurements with respect to the distance and render the system observable.

The main limits of the proposed approach mainly consist in the necessity of performing a parameter tuning of the model which, in this paper, has been performed a posteriori by considering the best matching of the model with the measured data. Additionally, some parameters in the algorithms, like the standard deviation of the change in the velocity, should be properly calibrated on a rough knowledge of the expected tag motion (e.g., maximum expected acceleration) to obtain satisfactory performances. In a future work, some of these physical and algorithmic parameters could be estimated by, e.g., enlarging the set of possible hypotheses or tuned by resorting to some adaptive rule. Finally, in this paper, a unidimensional problem has been addressed. In future works, more general motions can be considered.

References

[1] R. E. Martínez-Castro, S. Jang, J. Nicholas, and R. Bansal, "Experimental assessment of an RFID-based crack sensor for steel structures," *Smart Mater. Struct.*, vol. 26, no. 8, 2017, Art. no. 85035.

[2] R. P. E. Martínez-Castro and S. Jang, "Crack sensor using commercial UHF RFID technology for metallic structures," presented at Struct. Congr. Bridges, Non-Building Special Struct. Nonstruct. Compon., 2019.

[3] A. Motroni, A. Buffi, and P. Nepa, "A survey on indoor vehicle localization through RFID technology," *IEEE Access*, vol. 9, pp. 17921–17942, 2021, doi: 10.1109/ACCESS.2021.3052316.

[4] Y. Zhao, X. Zhao, L. Li, X. Liu, and Q. Li, "Timing: Tag interference modeling for RFID localization in dense deployment," *IEEE Sensors J.*, vol. 22, no. 23, pp. 23464–23475, Dec. 2022, doi: 10.1109/JSEN.2022.3215173.

[5] X. Yi, C. Cho, J. Cooper, Y. Wang, M. Tentzeris, and R. Leon, "Passive wireless antenna sensor for strain and crack sensing—Electromagnetic modeling, simulation, and testing," *Smart Mater. Struct.*, vol. 22, no. 8, 2013, Art. no. 85009.

[6] Y. He, M. M. Li, G. C. Wan, and M. S. Tong, "A passive and wireless sensor based on RFID antenna for detecting mechanical deformation," *IEEE Open J. Antennas Propag.*, vol. 1, pp. 426–434, 2020.

[7] A. Di Natale, A. Di Carlofelice, and E. Di Giampaolo, "A crack mouth opening displacement gauge made with passive UHF RFID technology," *IEEE Sensors J.*, vol. 22, no. 1, pp. 174–181, Jan. 2022, doi: 10.1109/JSEN.2021.3130064.

[8] A. Gregori, E. Di Giampaolo, A. Di Carlofelice, and C. Castoro, "Presenting a new wireless strain method for structural monitoring: Experimental validation," *J. Sens.*, vol. 2019, pp. 1–12, Nov. 2019, doi: 10.1155/2019/5370838.

[9] E. Di Giampaolo, A. Di Carlofelice, and A. Gregori, "An RFID-enabled wireless strain gauge sensor for static and dynamic structural monitoring," *IEEE Sensors J.*, vol. 17, no. 2, pp. 286–294, Jan. 2017, doi: 10.1109/JSEN.2016.2631259.
[10] S. Caizzone, E. Di Giampaolo, and G. Marrocco, "Constrained pole-zero synthesis of phase-oriented RFID sensor antennas," *IEEE Trans. Antennas Propag.*, vol. 64, no. 2, pp. 496–503, Feb. 2016, doi: 10.1109/TAP.2015.2511788.
[11] S. Caizzone and E. Di Giampaolo, "Wireless passive RFID crack width sensor for structural health monitoring," *IEEE Sensors J.*, vol. 15, no. 12, pp. 6767–6774, Dec. 2015, doi: 10.1109/JSEN.2015.2457455.
[12] S. Caizzone, E. DiGiampaolo, and G. Marrocco, "Wireless crack monitoring by stationary phase measurements from coupled RFID tags," *IEEE Trans. Antennas Propag.*, vol. 62, no. 12, pp. 6412–6419, Dec. 2014, doi: 10.1109/TAP.2014.2360553.
[13] E. Di Giampaolo and F. Martinelli, "A multiple baseline approach to face multipath," *IEEE J. Radio Freq. Identif.*, vol. 4, no. 4, pp. 314–321, Dec. 2020, doi: 10.1109/JRFID.2020.3022576.
[14] J. D. Kraus and R. J. Marhefka, *Antennas for All Applications*. New Delhi, India: Tata McGrawHill, 2003.
[15] E. Di Giampaolo, F. Martinelli, and F. Romanelli, "Exploiting the electromagnetic coupling to estimate the close motion of UHF-RFID tagged objects," in *Proc. IEEE 13th Int. Conf. RFID Technol. Appl. (RFID-TA)*, Aveiro, Portugal, 2023, pp. 201–204, doi: 10.1109/RFID-TA58140.2023.10290247.
[16] F. Martinelli and F. Romanelli, "A SLAM algorithm based on range and bearing estimation of passive UHF-RFID tags," in *Proc. 11th IEEE Int. Conf. RFID Technol. Appl. (IEEE RFID-TA)*, Oct. 2021, pp. 20–23.
[17] E. Di Giampaolo and F. Martinelli, "Range and bearing estimation of an UHF-RFID tag using the phase of the backscattered signal," *IEEE J. Radio Freq. Identif.*, vol. 4, no. 4, pp. 332–342, Dec. 2020, doi: 10.1109/JRFID.2020.3016168.
[18] S. J. Julier and J. K. Uhlmann, "Unscented filtering and nonlinear estimation," *Proc. IEEE*, vol. 92, no. 3, pp. 401–422, Mar. 2004, doi: 10.1109/JPROC.2003.823141.
[19] T. Boroushaki, I. Perper, M. Nachin, A. Rodriguez, and F. Adib, "RFusion: Robotic grasping via RF-visual sensing and learning," in *Proc. 19th ACM Conf. Embedded Netw. Sens. Syst.*, New York, NY, USA, pp. 192–205. [Online]. Available: https://doi.org/10.1145/3485730.3485944
[20] R. Carotenuto, M. Merenda, D. Iero, and F. G. D. Corte, "Ranging RFID tags with ultrasound," *IEEE Sensors J.*, vol. 18, no. 7, pp. 2967–2975, Apr. 2018, doi: 10.1109/JSEN.2018.2806564.
[21] A. Buffi, P. Nepa, and F. Lombardini, "A phase-based technique for localization of UHF-RFID tags moving on a conveyor belt: Performance analysis and test-case measurements," *IEEE Sensors J.*, vol. 15, no. 1, pp. 387–396, Jan. 2015.
[22] T. Deyle, C. J. Tralie, M. S. Reynolds, and C. C. Kemp, "In-hand radio frequency identification (RFID) for robotic manipulation," in *Proc. IEEE Int. Conf. Robot. Autom.*, Karlsruhe, Germany, 2013, pp. 1234–1241, doi: 10.1109/ICRA.2013.6630729.
[23] B. Friedlander, "Localization of signals in the near-field of an antenna array," *IEEE Trans. Signal Process.*, vol. 67, no. 15, pp. 3885–3893, Aug. 2019, doi: 10.1109/TSP.2019.2923164.
[24] "Beontag." Dec. 2023. [Online]. Available: https://www.lab-id.com/

Lorenzo Bianchi was born in Frosinone, Italy, in 1993. He received the B.S. degree (cum laude) in computer science engineering from the University of Rome Tor Vergata, Italy, in 2015, and the M.S. degree (cum laude) in robotics and automation engineering from the University of Pisa, Italy, in 2019.

In 2021 he attended a first-level Master about Design, Application, Regulation of Unmanned Aerial Vehicles and, since 2022 he has been a Ph.D. Student in computer science, control, and geoinformation with the University of Rome Tor Vergata, working mostly on autonomous drones and ground rovers. His research interests include SLAM, visual SLAM, robot localization, and deep learning.

Emidio Di Giampaolo received the Laurea degree in electronic engineering and the Ph.D. degree in applied electromagnetics from the University of L'Aquila, Italy, in 1994 and 1998, respectively.

From 1998 to 2004, he has been a Postdoctoral Researcher with the University of L'Aquila. In the spring of 2000, he was a Visiting Researcher with the European Space Research and Technology Centre, Noordwijk, The Netherlands. From 2005 to 2009 he was a Researcher with the University of Rome Tor Vergata. Since 2010, he is with the University of L'Aquila as an Associate Professor. His research interests mainly concern numerical methods for modeling radio-wave propagation in complex environments, antennas and radio localization.

Francesco Martinelli was born in Rome, Italy, in 1969. He received the Laurea degree (cum laude) in electrical engineering and the Ph.D. degree in computer science and automation engineering from the University of Rome Tor Vergata, Italy, in 1994 and 1998, respectively, where he is currently an Associate Professor.

In 1997, he was a Visiting Scholar with the Department of Manufacturing Engineering, Boston University, MA, USA. His research interests include mobile robot localization, dynamic scheduling of manufacturing systems, and filtering methods.

Fabrizio Romanelli was born in Viterbo, Italy, in 1979. He received the B.S. and M.S. degrees in automation engineering from the University of Rome, Tor Vergata, in 2005.

From 2006 to 2017, he was a Robotics Specialist and a Software Manager with the Research & Development Department, Comau Robotics S.p.A., Turin, Italy. From 2017 to 2019, he was a Research Engineer with the Advanced Robotics Research Line designing the software architecture for legged robots, Istituto Italiano di Tecnologia, Genoa, Italy. He is a Ph.D. Candidate in computer science, control and geoinformation with the University of Rome, focusing on robotic perception and sensor fusion techniques. He holds two patents. He is a Author of 28 articles and 1 book chapter. His research interests include resilient robotic perception, deep learning, sensor fusion techniques, simultaneous localization and mapping, and visual SLAM.

Open Access funding provided by 'Università degli Studi dell'Aquila' within the CRUI CARE Agreement